RESEARCH IN APPLIED GEOPHYSICS

REPORT NO. 3

QUANTITATIVE INTERPRETATION OF INPUT AEM MEASUREMENTS

BY

G. J. PALACKY AND G. F. WEST

Reprinted for private circulation from
GEOPHYSICS
Vol. 38, No. 6, December, 1973

QUANTITATIVE INTERPRETATION OF INPUT AEM MEASUREMENTS†

G. J. PALACKY* AND G. F. WEST‡

Recent improvements of the INPUT airborne electromagnetic system have made possible a more quantitative approach to interpretation. The necessary interpretational aids can be obtained in two ways: either by correlating the system and ground EM measurements, or by devising computational or analog quantitative models. Both approaches have been explored. In the former, the system decay rate can be correlated with the apparent conductivity-thickness (σt) estimated by ground surveys. In the latter, four quantitative models were investigated, vertical half-plane, vertical ribbon, dipping half-plane, and homogeneous half-space. Nomograms have been constructed which make it possible to determine σt, conductor depth, and dip for sheet-like conductors, and conductivity for a homogeneous half-space. Field examples show that this procedure can be used satisfactorily in the routine interpretation of records obtained by this system.

INTRODUCTION

INPUT[1] (hereinafter referred to simply as the system) is a towed-bird, time-domain AEM system whose first version was constructed by A. R. Barringer in the late 1950's. Currently, it is the most widely used AEM system; 160,000 miles of surveys were flown in 1972. Its principle is explained in Figure 1.

Brief description of the system

The primary magnetic field is generated by current pulses which are 1.1 msec long and alternate in polarity. The emf due to the secondary magnetic field is measured at six time gates (0.26, 0.48, 0.75, 1.10, 1.57, and 2.10 msec) after the transmitter switch-off. The amplitude is averaged over a time interval which is increased from 0.22 msec to 0.54 msec.

The presence of a conductor in the ground generates in the receiver an induced emf which is superimposed upon the primary signal and distorts it, but subsequently which appears uniquely as a decaying signal following the cessation of the primary pulse.

The transmitter is formed by a horizontal loop wound around the aircraft. To make its area as large as possible, it is fixed at the wing tips and the rudder. The receiver coil is oriented with its axis horizontal, approximately in the direction of the primary magnetic field vector. The nominal position of the bird containing the receiver is 350 ft behind and 200 ft below the aircraft. The nominal flight height of the aircraft is 400 ft and the usual flight speed is 120 mph.

Continuous records of the six secondary signal amplitudes are generated by averaging the single pulses over several transmitter periods. A simple exponential averaging with a time constant of 0.5 sec is employed in the currently used system (Mk VI). A more elaborate four-pole active filter with a time constant of 5 sec was used in Mk V. Mk VI, which became operational in 1972, is considered in this paper, if not stated otherwise.

Interpretation

Two courses of action are open in the search for a more quantitative interpretation procedure. One possibility is to extend the existing qualitative approach: the type of response generated by

[1] Registered Trademark of Barringer Research Ltd.

† Manuscript received by the Editor February 8, 1973.

* Now with Barringer Research Limited, Rexdale, Ontario, Canada M9W 5G2; formerly, University of Toronto, Ontario, Canada, M5S 1A7.

‡ University of Toronto, Toronto, Ontario, Canada M5S 1A7.

© 1973 Society of Exploration Geophysicsts. All rights reserved.

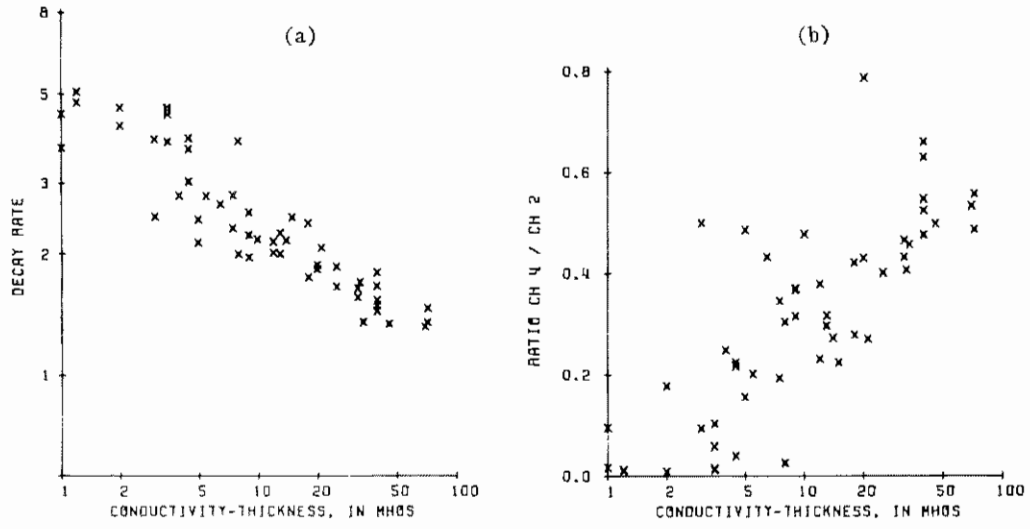

FIG. 4. Correlation of ground EM and measurements of the system. Ground σt was determined from the horizontal-loop EM measurements using phasor diagrams. It is correlated to (a) the decay rate of the exponential model fitted at the anomaly peak, and (b) amplitude ratios of channels 4 to 2.

nels 1 and 5, and lower on 2, 3, and 4. The major departure on channel 6 is not significant in absolute terms because logarithmic differences are plotted. The bias for the power law is opposite. The measured channel 1 is low compared with approximation; channels 2, 3, and 4 are high; and 6 is low.

The system's records (Mk V) and the result of the subsequent ground checks in two areas of the Canadian Precambrian Shield were made available by the Société Québecoise d'Exploration Minière. An attempt was made to correlate the two data sets. The ground measurements employed the horizontal-loop EM method. Most of the ground checks revealed conductive zones of substantial strike length and limited width. Phasor diagrams of response amplitude, based on a vertical half-plane or dipping half-plane model (Grant and West, 1965) were used in the quantitative interpretation of such anomalies, which were presumably caused by dike-like bodies. With this procedure, the conductivity-thickness (σt) of the conductive zones can be estimated. As Parasnis (1971) has pointed out, there are many circumstances that can make such an estimate inaccurate, particularly if conductive overburden is present. Therefore, the σt estimates from the ground surveys are only rough estimates of the true σt, perhaps reliable to within a factor of two in the majority of cases. Another difficulty arises from matching the location of airborne and ground anomalies. This can seldom be achieved perfectly and the true σt may change significantly along the strike of a conductor.

Figure 4a shows the correlation between ground σt and the exponential decay rate. A similar correlation, although slightly more scattered, was found for the power law decay rate. The decay rate which uses information available on all channels is a better parameter than channel ratios (Figure 4b).

MODELING OF THE SYSTEM'S RESPONSE

Most theoretical and model studies for the system have been made in the frequency domain. An exception is a recent paper by Becker et al (1972) which describes model measurements in the time domain. In principle, if sets of frequency-domain data covering a broad frequency range are available, they can be converted to the time domain by performing a Fourier transformation. The tabulation of the secondary fields due to an alternating dipole source situated over a layered conducting half-space, made by Frischknecht (1967), has served for the computation of the time-domain response in two papers. Nelson and Morris (1969) obtained data for the homogeneous half-space and a layer over the half-space. Their results are

given in the form of relative channel amplitudes versus conductivity. Becker (1969) has obtained similar results for the homogeneous half-space and a thin horizontal sheet. His results are in the form of decay curves showing the change with delay time of the instantaneous emf induced in the receiver after cessation of the transmitter pulse.

Computations of system response over thin conductive dikes are not available because no suitable theoretical solution is possible except for infinite frequency, but this is not useful for the transformation to the time domain. Ghosh and West (1971) completed an atlas of frequency-domain master curves for several AEM systems over thin dike conductors by analog modeling. The results are available only for a limited number of induction numbers and the accuracy is limited by a measurement error. These two facts had to be considered before transforming their data to the time domain.

Transformation of frequency-domain results to the time domain

A computational scheme for obtaining system amplitudes C_k, $k=1, 2, \cdots 6$ from the frequency-domain analog data is shown in Figure 5. The inputs are the real and imaginary parts of the secondary field intensity F_n (expressed as a fraction of the primary field intensity) for n values of frequency (expressed in combination with σt of the conductor). A continuous function notation, such as $x(t)$, $G(\omega)$, is used when the number of points is determined by the computational feasibility. If it is limited for other reasons, the discrete notation such as C_k, F_n is used.

For a reliable computation of the Fourier transformation, a sufficient number of points of the function $G(\omega)$, derived from F_n, had to be obtained. The analog model measurements were made only for ten or fewer induction numbers. $G(\omega)$ was therefore obtained from a cubic spline interpolation (Greville, 1964) of F_n. For this interpolation, it was assumed that no error existed in the values of F_n. Thus, the interpolated curve is forced to pass through each point F_n. Due to the measurement error, this assumption was not always correct and undulations sometimes occurred in $G(\omega)$ in the vicinity of less reliable points of F_n. The in-phase and quadrature components were measured and interpolated separately even though

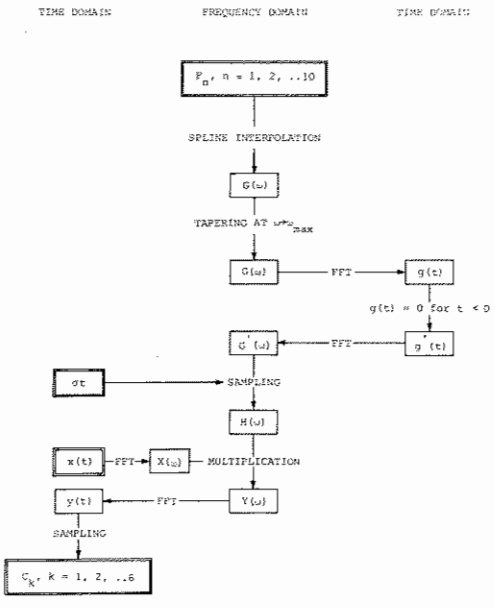

FIG. 5. Flow chart showing the procedure used for transformation of frequency-domain analog model measurements to the time domain.

they are not independent. A correction scheme was then constructed to rectify this situation.

The physical system is real and realizable, i.e., the time-domain system function $g(t)$ corresponding to $G(\omega)$ has no imaginary part and vanishes for $t<0$. Thus, the real part of $G(\omega)$ is an even function and the imaginary part is odd. Because of this symmetry, if separate inverse transforms are taken of the real and imaginary parts,

$$r(t) = \mathfrak{F}^{-1}[R(\omega)] = \mathfrak{F}^{-1}[\mathrm{Re}\ G(\omega)]$$

and

$$s(t) = \mathfrak{F}^{-1}[S(\omega)] = \mathfrak{F}^{-1}[\mathrm{Im}\ G(\omega)], \quad (5)$$

then $r(t)$ must be purely real and $s(t)$ purely imaginary. Also, because $R(\omega)$ and $S(\omega)$ are themselves real functions, $r(t)$ and $s(t)$ must have even real parts and odd imaginary parts, respectively. Since

$$\begin{aligned} G(\omega) &= R(\omega) + iS(\omega), \\ g(t) &= r(t) + is(t), \end{aligned} \quad (6)$$

and

$$\begin{aligned} r(t) &= is(t) \qquad t < 0, \\ r(t) &= -is(t) \qquad t > 0. \end{aligned} \quad (7)$$

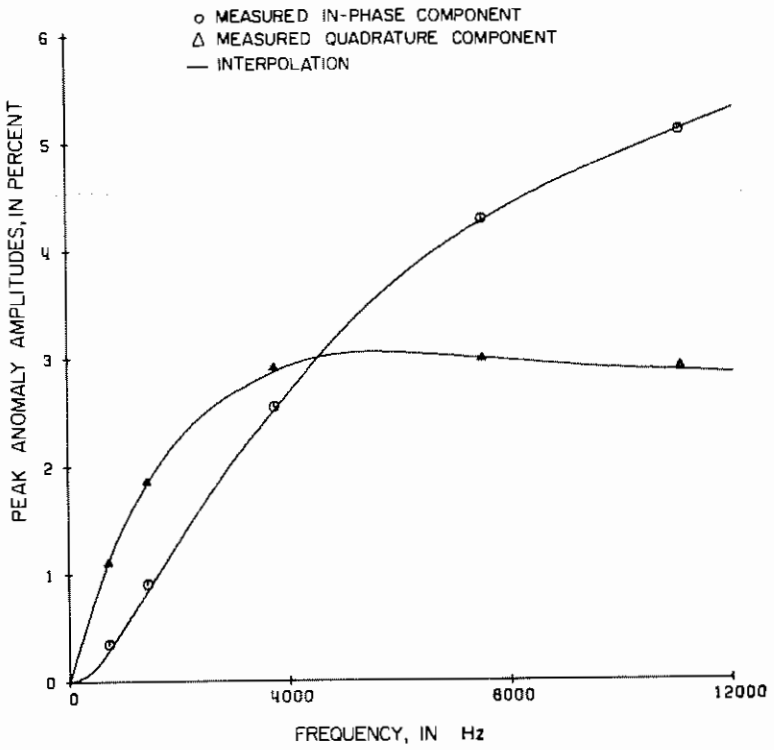

FIG. 6. The continuous function $G'(\omega)$ was obtained from the model measurements $F_n(n=1, \cdots, 10)$ by the procedure shown in Figure 5.

The procedure adopted, therefore, was to take inverse transforms of the in-phase and quadrature frequency response separately to see if $r(t)=s(t)$. The observed differences were less than 10 percent. The errors were minimized by averaging $-is(t)$ with $r(t)$. The corrected values are denoted $r'(t)$ and $s'(t)$. In finding $s(t)$, a window function was applied to $S(\omega)$ to prevent aliasing effects which otherwise were apparent even after taking 4000 harmonics for the transformation.

After windowing in the frequency domain and averaging in the time domain, any undulations present in $G(\omega)$ disappeared in $G'(\omega)$ because the new function is not forced to go exactly through all F_n points. An example of the peak frequency-domain response over a vertical half-plane at a flight height of 385 ft, is shown in Figure 6. The effects of forcing $g(t)$ to be realizable are apparent.

The secondary received signal $y(t)$, in the time domain, can be expressed as a convolution of the primary field signal $x(t)$ and the system function $g(t)$ characterizing the ground response. $x(t)$ was taken as a sine pulse, the duration of which was 1.1 msec and amplitude unity. The convolution can be computed more conveniently as a multiplication in the frequency domain

$$Y(\omega) = X(\omega) \cdot H(\omega). \tag{8}$$

$H(\omega)$ is taken from $G'(\omega)$ after rescaling for different σt values. For this Fourier transformation, 256 values of $H(\omega)$ have been found sufficient. The Cooley-Tukey (1965) algorithm for fast Fourier transform has been used. All secondary fields have been expressed as fractions of the zero-to-peak primary-field signal at the receiver.

To obtain the system channel amplitudes C_k, $k=1, 2, \cdots 6$, the secondary magnetic field $y(t)$ is sampled and averaged over each of the six time intervals

$$C_k = 1/(NR_k - NL_k + 1) \sum_{i=NL_k}^{NR_k} y(t_i), \tag{9}$$

where NR_k, NL_k are the limits of the time gate in msec.

THIN SHEET MODELS

Vertical half-plane profiles

The results of analog model measurements by Ghosh and West (1971) were transformed to the time domain using the procedure outlined in the previous section. The frequency-domain profiles were available for ten induction numbers. The time-domain profiles are shown for two flight heights, 385 and 462 ft, and 3 values of σt (Figure 7).

The average anomaly half-width is 300 ft. It varies only slightly with σt, but increases with the flight height. The amplitude changes will be described in the next section. A comparison of model and field profiles can be made only for Mk VI measurements because the shapes of anomalies are distorted on Mk V records, due to the heavy nonlinear smoothing.

The small peak followed by a large one is typical for anomalies due to vertical half-plane conductors. In practice, however, the peaks were frequently marked as two separate conductors by some interpreters. Not surprisingly, the anomaly corresponding to the smaller peak could not be detected in the ground follow-up measurements. A comparison of a model profile and Mk VI record is in Figure 8. The survey was flown over the Staunton Cu-Zn ore deposit in Quebec.

Vertical half-plane amplitudes

As long as quantitative interpretation is made without a digital computer, the evaluation of several parameters is more practicable than matched filtering. The dependence of anomaly

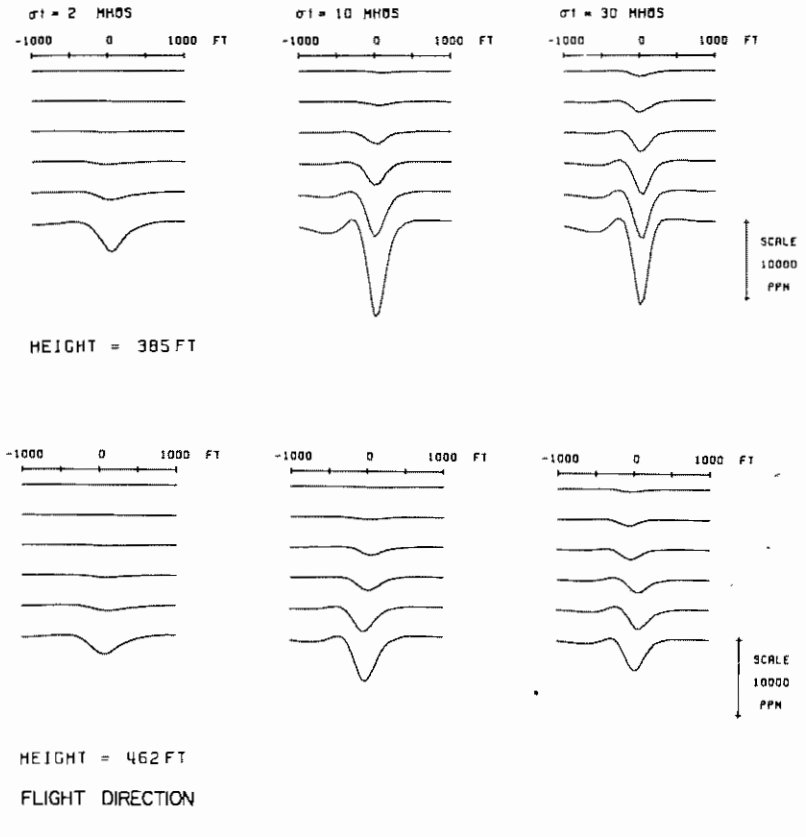

FIG. 7. Model profiles over a vertical half-plane of given σt. The flight height was 385 and 462 ft and the conductor was located at zero depth. Note the minor peak before the anomaly center.

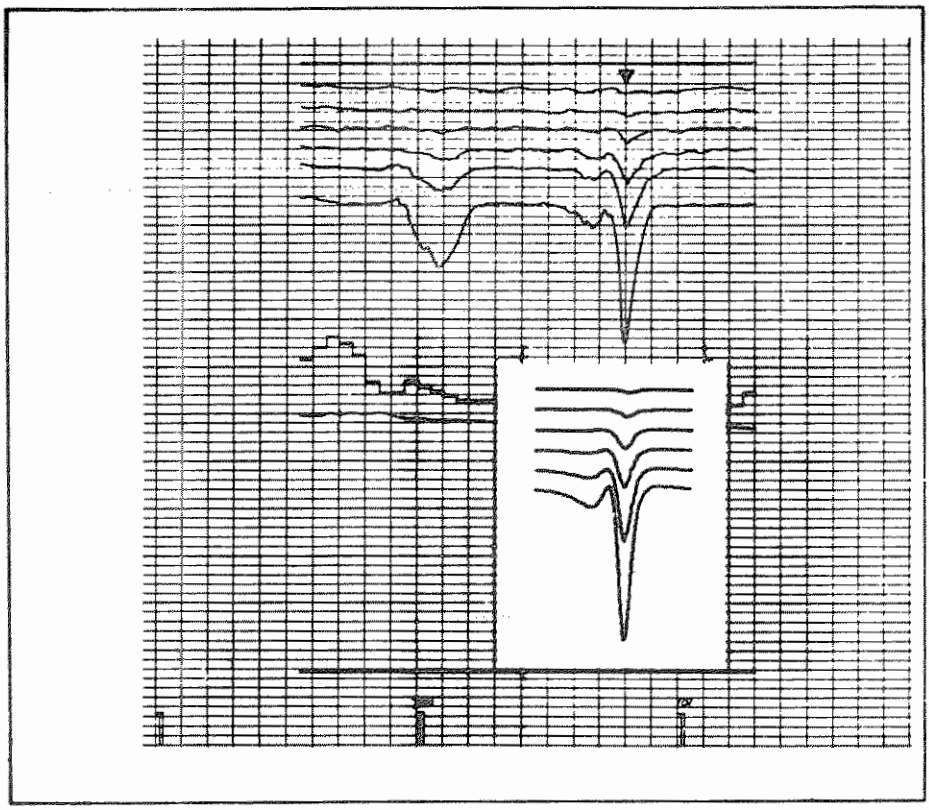

FIG. 8. A system record over the Cu-Zn deposit Staunton, Québec, is compared with a model curve over a vertical half-plane (flight height, 385 ft: $\sigma t = 10$ mhos). The outcropping deposit is 700 ft long and 5.5 ft wide.

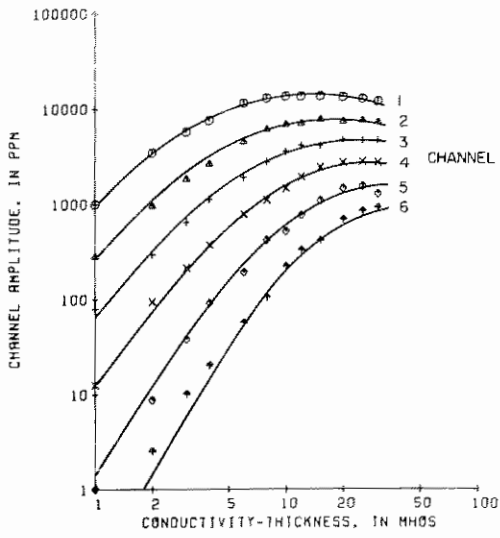

peak amplitude on σt was studied first. Figure 9 shows results of the transformation to the time domain. The deviations from the smoothed curve are due to errors in model measurements, spline interpolation in the frequency domain, and inaccuracies in the transformation. The smoothed curves are shown in Figure 10. The channel amplitudes rise rapidly with σt, reach a maximum of 11,000 ppm on channel 1, for $\sigma t = 10$ mhos, and slowly decrease.

Next the change of anomaly amplitudes with conductor depth was studied (Figure 11, channel

FIG. 9. Example of data on which the interpretation nomogram (Figure 10) is based. The transformation to the time-domain was made for 12 values of σt in one run. These values (circles, triangles, etc.) were then interpolated by hand.

2 shown). The frequency-domain measurements were available at five different flight heights (385, 462, 578, 770, and 1039 ft). Because the model was placed in a free space, the change in flight height and the change in conductor depth are equivalent. For convenience in discussion, the standard flight height of 400 ft will be assumed and all changes in amplitude will be considered due to changes of conductor depth. The decrease of amplitude with depth depends strongly on σt. It is slower for poor conductors; a 2.7th power for $\sigma t = 1$ mho, a 5th power for $\sigma t = 50$ mhos. Because of its effect on the response fall-off with depth, it is desirable that σt is estimated before any correction to amplitude for flight height is made.

After computing the channel amplitudes for conductor depths in the complete range of σt, it was found that within the data accuracy all the curve sets can be matched by shifting them along the σt and channel amplitude axes. The amount of shift required is shown in Figure 10 in the form of a grid near the upper edge of the illustration. This permits the use of Figure 10 as a nomogram in the following way: The six channel amplitudes for an anomaly should be plotted on a tracing paper along the vertical logarithmic scale given on the right-hand side. The 100,000 ppm point must also be marked. Then the set of points should be fitted to the curve family by shifting in both vertical and horizontal directions, but without rotation. The position of the 100,000 ppm mark on the upper grid will indicate the value of σt and conductor depth. The vertical scale may be recalibrated in millimeters of the records using the equivalence 1 mm = 100 ppm for the Mk VI (Wondergem, 1971).

Vertical ribbon

For the vertical ribbon model (a thin sheet having finite dip extent and infinite strike length),

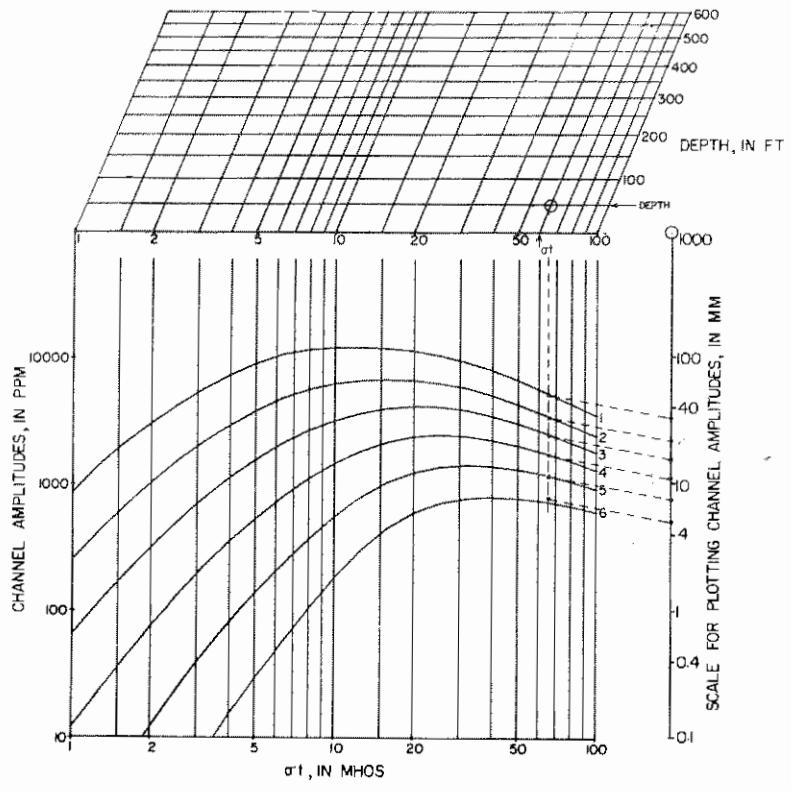

FIG. 10. Nomogram for estimation of σt and conductor depth. The peak anomaly amplitudes are plotted on an overlay using the "scale for plotting." The array of points is then fitted to the curve family. The position of the circle in the upper grid indicates the values of the interpreted parameters.

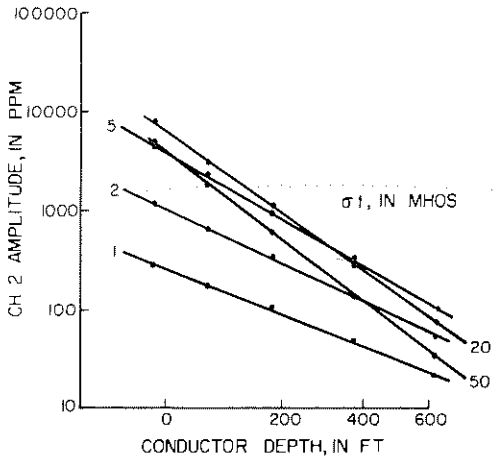

FIG. 11. The decrease of channel amplitudes with conductor depth obeys a power law: the power changes from 2.7 for $\sigma t = 1$ mho to 5 for $\sigma t = 50$ mhos.

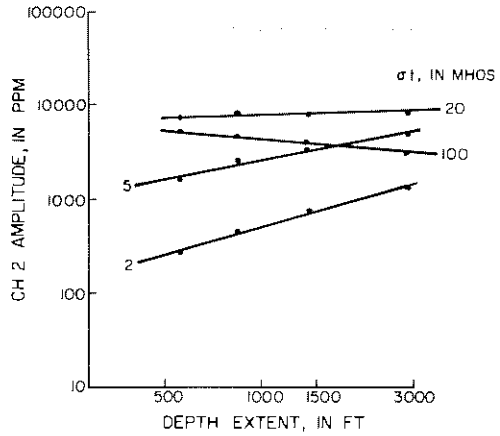

FIG. 12. The change of channel amplitudes with depth extent depends on σt. The lines should not be extrapolated for a depth extent of less than 500 ft.

the amplitude depends on the depth extent (Figure 12). The model measurements were conducted for four depth extents (587, 880, 1467, and 2934 ft, the last being nearly identical to the vertical half-plane). The model data were available for only five induction numbers and the reliability of transformation is lower than in the previous experiments. The anomaly amplitude increases markedly with increasing depth extent for poor conductors, but much less so for good ones. The change obeys approximately a power law for the depth extents between 500 and 3000 ft. This relationship must not, however, be extrapolated to depth extents smaller than 500 ft because the amplitude starts to decrease more rapidly and does not obey a simple power law.

The depth extent cannot be determined from an AEM survey alone as an additional piece of geologic or geophysical information is required. In most cases, it is not worthwhile to consider the ribbon model a priori.

Becker et al (1972) have made a number of time-domain model measurements for this system. Their work was less extensive than the model work of Ghosh and West (1971) and the channel gates do not quite correspond to the actual system. Their results, seven values of σt versus amplitude at 0.5 msec, are shown in Figure 13 matched to the channel 2 curve from Figure 10 which was corrected for a finite depth extent. The agreement is reasonably good. The flight height, 450 ft, agrees well with the value of 440 ft found from our nomogram. However, according to our data, Becker's (1972) plate model was not quite large enough to simulate a vertical half-plane as it had a scaled depth extent of only 780 ft.

Dipping half-plane

The unique anomaly shape (Figure 7) consisting of minor peak, saddle, and major peak suggests the use of the ratio of the two amplitudes in interpretation. The model data shows that this

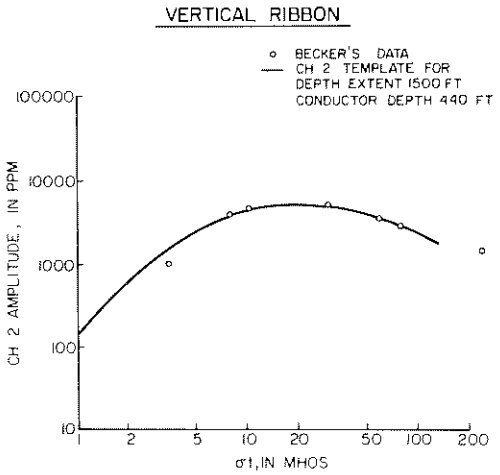

FIG. 13. Comparison of the time domain measurements by Becker et al (1972) with a curve, σt versus channel 2 amplitude from Figure 10, corrected for a finite depth extent.

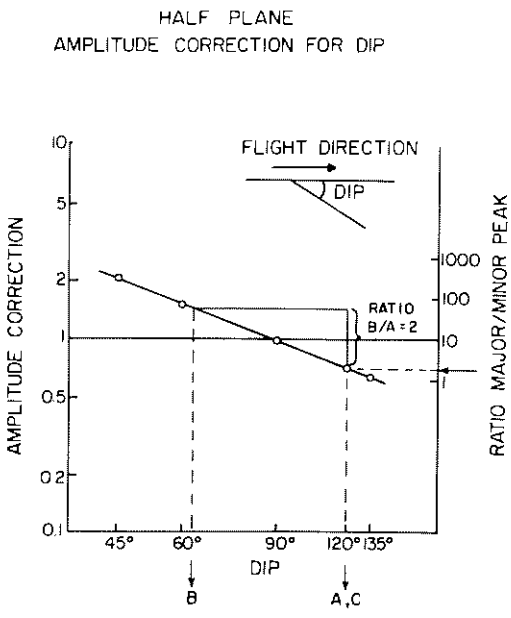

FIG. 14. Dip of a half-plane can be estimated from the ratio of "major" to "minor" peak amplitude. Anomalies A, B, C from Figure 15 demonstrate the use of the graph. Because of the strong effect of dip on anomaly amplitude, a correction (using the left-hand scale) has to be made before estimating conductor depth.

ratio depends on the dip of the half-plane model (Figure 14). The frequency-domain model measurements were made for dips 45, 60, 90, 120, and 135 degrees. The angle increases clockwise. The ratio for a vertical half-plane is 10; for 135 degrees it decreases to 1.5. Two distinctive peaks are observed in updip flights. The second indicates the conductor's upper edge. In the opposite direction, only one peak with much larger amplitude is recorded.

The dip determination is demonstrated on a field example from northern Manitoba. An Mk VI survey was conducted in 1972 in an area covered by 50–100 ft of moderately conductive overburden. Most of the conductors are dipping graphitic bands. Three parallel profiles (A, B, C) 1200 ft apart are shown in Figure 15. The flight direction was north–south on A and C, south–north on B. As expected for a dipping conductor, two peaks are on profiles A and C and only one on B. The ratio of the two peak amplitudes is 2.1 on A and 1.9 on C. A dip of 120 degrees is obtained from the graph in Figure 14. An independent dip estimate can be made from the ratio of peak amplitudes on profiles flown in the opposite direction. By comparing the amplitudes on profiles A and B, a ratio of 2 is obtained

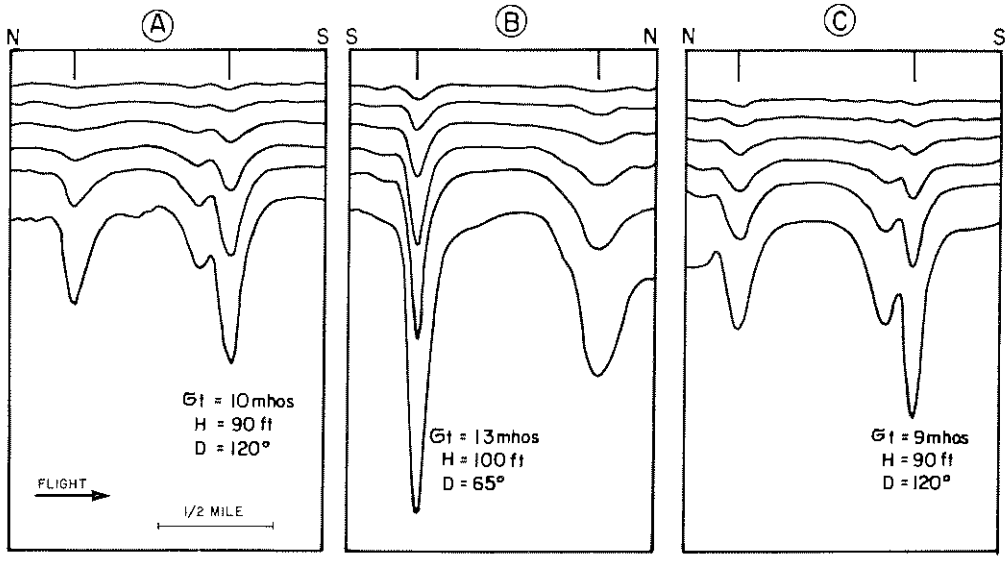

FIG. 15. An example of a dipping conductor. Profile B was flown in opposite direction to A and C. All three profiles indicated approximately the same dip σt and depth.

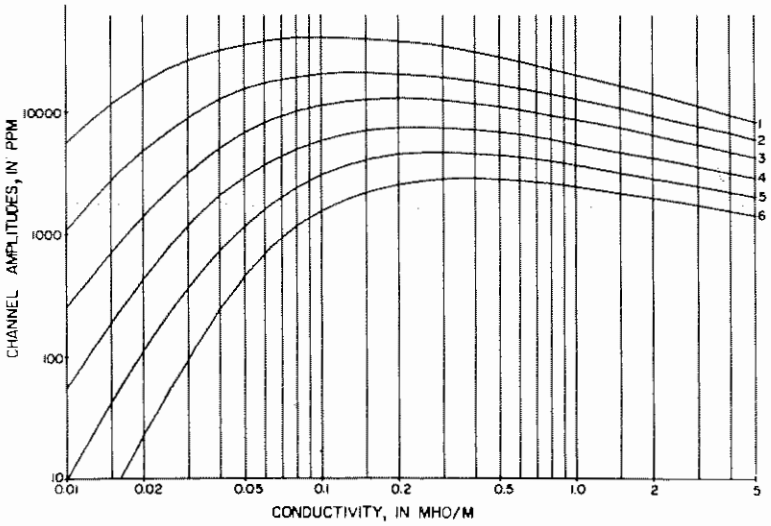

FIG. 16. Graph for estimation of conductivity for a homogeneous half-space model.

from which a dip of 65 degrees on profile B can be estimated.

As discussed in the previous section, the peak amplitudes are used for a depth estimate. It is necessary to make the dip determination and amplitude correction before attempting a depth estimate. The corrections can be read from Figure 14. The amplitude correction is 1.4 for the example shown. The values of σt and conductor depth were estimated for the three anomalies shown in Figure 15. Without the amplitude correction for dip, a depth of 130 ft would have been estimated on profiles A and C and 50 ft on B.

HOMOGENOUS HALF-SPACE MODEL

In the previous computations of the system response over a homogeneous half-space (Nelson and Morris, 1969; Becker, 1969), the channel amplitudes either were not computed or given in relative units. However, a knowledge of actual amplitudes (in ppm) is essential. Instead of going again to Frischknecht's tables (1967), the frequency-domain system response was computed using the method of Lajoie et al (1972). The results were transformed to the time domain using the same procedure as applied to the model data.

First, the change of channel amplitudes with conductivity was studied in the range 0.01 to 5 mho/m (Figure 16). For poor conductors, the amplitudes rise rapidly with conductivity, reach a maximum of 35,000 ppm on channel one for $\sigma = 0.1$ mho/m and then slowly decrease. The maximum is about three times larger than for the vertical half-plane model.

While in the previous chapters the analysis has been made for anomaly peaks, the anomaly shape is of no interest for the half-space model. Because the conductive zone is infinitely extensive in all directions, the only dimension which can affect the amplitude is the flight height (or equivalently, the conductor depth). The computations were made for depths 0, 150, 300, and 450 ft assuming a standard flight height of 400 ft. The decrease of amplitude with depth (Figure 17, channel 2 shown) depends on the conductivity and clearly obeys a power law. A dependence on σ was suspected by Becker (1969), but was not clearly demonstrated. For $\sigma = 0.1$ mho/m, the amplitude decreases with 2.2nd power, increasing to 3 for $\sigma = 5$ mho/m. In comparison, the maximum amplitude decrease with increasing σt for the vertical half-plane model was with the fifth power.

The number of bodies which can be realistically approximated by a homogeneous half-space model is rather limited. Only the sea or large deep lakes fall into this category. The dependence of system amplitudes on flight height was studied in a test flight over Lake Ontario. The survey was made by Questor Surveys Ltd. in November,

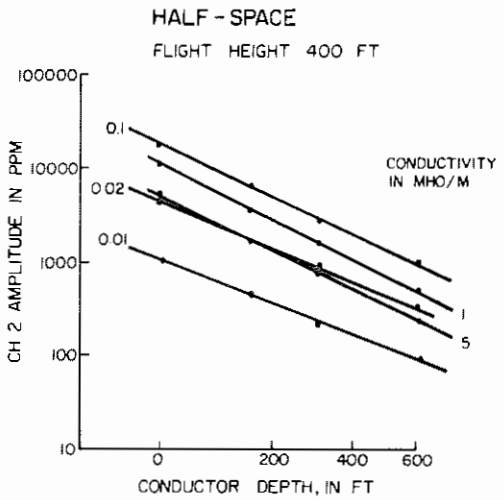

FIG. 17. Channel amplitudes decrease with the conductor depth according to a power law. Unlike the vertical half-plane model, the dependence on conductivity is not very significant.

1971. The flight height was between 380 and 540 ft. The 6 channel amplitudes are plotted on a logarithmic scale and compared with theoretical response of a homogeneous half-space (Figure 18, model A). The agreement in amplitude change is reasonably good, but there is a discrepancy in the absolute values of amplitudes. The system calibration is known to be 1 mm = 100 ppm and the measured amplitudes are about 50 percent smaller. By comparison with Figure 16, a conductivity of 0.1 mho/m was found. This value is significantly higher than that given in IJC Report (1969) for Lake Ontario ($\sigma = 0.035$ mho/m).

The likely explanation for the disagreement in amplitude and conductivity is that the homogeneous half-space is not a suitable model. It is evident from the geologic situation that the lake bottom is made of conductive Paleozoic shales. It is likely that in the surveyed area east of Toronto the water layer was not sufficiently thick (only about 100 ft). Therefore, another model (B) was considered. A response of a homogeneous half-space of $\sigma = 0.1$ mho/m overlain by a 100 ft layer of $\sigma = 0.035$ mho/m was computed. The two models are identical except for amplitude which is about 50 percent smaller (Figure 18).

In practice, the homogeneous half-space model may be used for the determination of conductivity of large tabular bodies. Anomalies are selected for interpretation according to their shape. A suitable anomaly which was recorded over a lake was interpreted using Figure 16. The conductivity estimate, $\sigma = 0.013$, mho/m is reasonable for unpolluted fresh water (Figure 19).

CONCLUSIONS

Several approaches to the quantitative interpretation of the system's measurements were discussed in this paper. In our opinion, the best procedure for a routine interpretation will consist of the following steps. First, the records are searched for anomalies and suitable quantitative models selected according to the anomaly shape. A double peak pattern is typical for the dipping sheet conductors. The ratio of the two peaks is used for a dip estimate and amplitude correction (Figure 14). The conductivity-thickness (σt) and conductor depth are determined from a nomogram (Figure 10) which is an equivalent of phasor

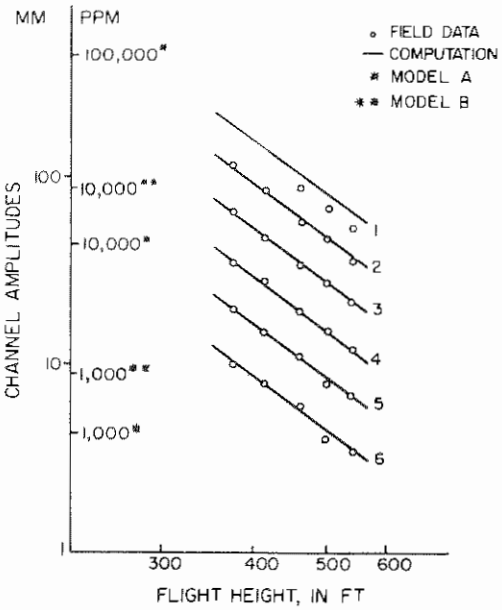

FIG. 18. Field data over Lake Ontario (circles, scale in mm) are compared with two theoretical models (solid line, scale in ppm). Model A is homogeneous half-space ($\sigma = 0.1$ mho/m), and model B is half-space ($\sigma = 0.1$ mho/m) overlain by a 100 ft thick layer ($\sigma = 0.035$ mho/m). Only the amplitudes differ, the rate of amplitude change with flight height remains unchanged.

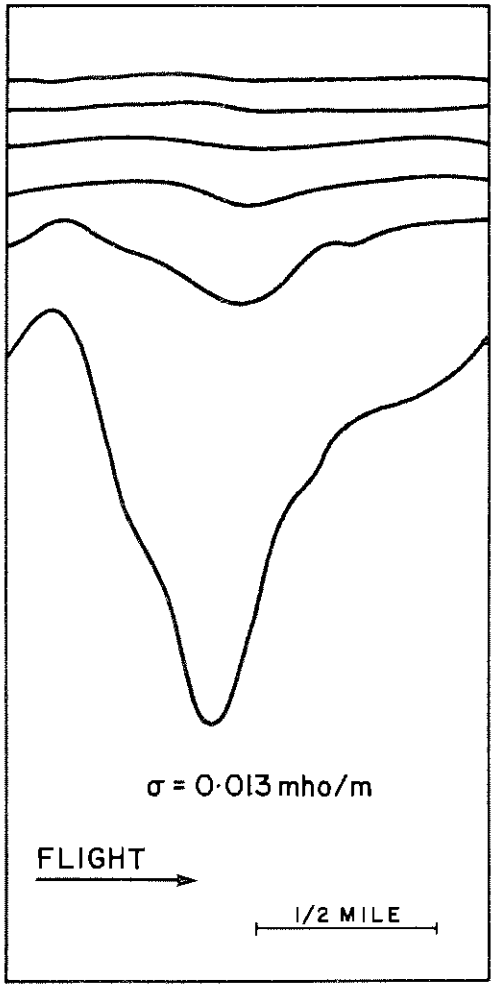

FIG. 19. An example of a large tabular conductor (fresh-water lake in northern Manitoba). The conductivity was estimated by a comparison with the homogeneous half-space model (Figure 16).

diagrams used for the interpretation of frequency domain EM measurements. An additional piece of geophysical information would be required for an estimate of the depth or strike extent. If an anomaly does not fit the thin sheet model and is very broad, the homogeneous half-space model (Figure 16) is used for a conductivity estimate. A digital computer can be used for most routine operations, such as anomaly recognition and parameter estimation. The necessary software has been developed and tested on field data (Palacky, 1972).

ACKNOWLEDGMENTS

Financial assistance from the National Research Council of Canada and Selco Exploration Ltd. is gratefully acknowledged, as well as scholarships to GJP from Kennecott Copper Corp. and University of Toronto in 1970–71. Many thanks are due to Société Québecoise Minière, Questor Surveys Ltd., and Barringer Research Ltd. for providing the field data.

REFERENCES

Becker, A., 1969, Simulation of time-domain, airborne electromagnetic system response: Geophysics, v. 34, p. 739–752.

Becker, A., Gavreau, C., and Collet, L. S., 1972, Scale model study of time domain electromagnetic response of tabular conductors: CIM Trans., v. 75, no. 725, p. 90–95.

Cooley, J. W., and Tukey, J. E., 1965, An algorithm for the machine computation of complex Fourier series: Math. Comput., v. 19, p. 297–301.

Frischknecht, F. C., 1967, Fields about an oscillating magnetic dipole over two layer earth: Quart. of the Colorado School of Mines, v. 62, no. 1.

Ghosh, M. K., and West, G. F., 1971, AEM analogue model studies: Toronto, Norman Paterson and Assoc.

Grant, F. S., and West, G. F., 1965, Interpretation theory in applied geophysics: New York, McGraw-Hill Book Co., Inc., p. 444–464.

Greville, T. N. E., 1964 Numerical procedures for interpolation by spline functions: J. SIAM Num. Anal., Ser. B., v. 1, p. 53–68.

IJC Report, 1969, Pollution of Lake Erie, Lake Ontario and the international section of the St. Lawrence Seaway: Toronto, International Joint Commission.

Lajoie, J., Alfonso-Roche, J., and West, G. F., 1972, EM Response of an arbitrary source on a layered earth; A new computational approach: Presented at the 42nd Annual International SEG Meeting, November 28, 1972, Anaheim, Calif.

Lazenby, P. G., 1972, Examples of field data obtained with the INPUT airborne electro-magnetic system: Toronto, Questor Surveys Limited, p. 1–28.

Mallick, K., 1972, Conducting sphere in electromagnetic input field: Geophys. Pros., v. 20, p. 293–303.

Nelson, P. H., 1973, Model results and field checks for a time-domain airborne EM system: Geophysics, v. 38, no. 5, p. 845–853.

Nelson, P. H., and Morris, D. B., 1969, Theoretical response of a time domain airborne electromagnetic system: Geophysics, v. 34, p. 729–738.

Palacky, G. J., 1972, Computer assisted interpretation of multi-channel airborne electromagnetic measurements: Ph.D. thesis, University of Toronto.

Palacky, G. J., and West, G. F., 1970, Computer anomaly recognition and classification: Presented at the 40th Annual International SEG Meeting, November 11, 1970, New Orleans, La.

Parasnis, D. S., 1971, Analysis of some multi-frequency multi-separation electromagnetic surveys: Geophys. Pros., v. 19, p. 163–179.

Paterson, N. R., 1971, Airborne electromagnetic methods as applied to search for sulphide deposits: CIM Trans., v. 74, p. 1–10.

Wagg, D. M., 1970, Airborne electromagnetic systems: Ottawa, Geoterrex Limited, p. 1–12.

Wondergem, H., 1972, Personal Communication.